ACS APPLIED MATERIALS & INTERFACES

Research Article

www.acsami.org

Zn_2SnO_4 Nanowires versus Nanoplates: Electrochemical Performance and Morphological Evolution during Li-Cycling

Christie T. Cherian, Minrui Zheng, M. V. Reddy, B. V. R. Chowdari, and Chorng Haur Sow*

Physics department, National University of Singapore, 2 Science Drive 3, Singapore, 117551

ABSTRACT: Zn_2SnO_4 nanowires have been synthesized directly on stainless steel substrate without any buffer layers by the vapor transport method. The structural and morphological properties are investigated by means of X-ray diffraction (XRD) and transmission electron microscopy (TEM). The electrochemical performance of Zn_2SnO_4 nanowires is examined by galvanostatic cycling and cyclic voltammetry (CV) measurements in two different voltage windows, 0.005−3 and 0.005−1.5 V vs Li and compared to that of Zn_2SnO_4 nanoplates prepared by hydrothermal method. Galvanostatic cycling studies of Zn_2SnO_4 nanowires in the voltage range 0.005−3 V, at a current of 120 mA g^{-1}, show a reversible capacity of 1000 (±5) mAh g^{-1} with almost stable capacity for first 10 cycles, which thereafter fades to 695 mAh g^{-1} by 60 cycles. Upon cycling in the voltage range 0.005−1.5 V vs Li, a stable, reversible capacity of 680 (±5) mAh g^{-1} is observed for first 10 cycles with a capacity retention of 58% between 10−50 cycles. On the other hand, Zn_2SnO_4 nanoplates show drastic capacity fading up to 10 cycles and then showed a capacity retention of 80% and 70% between 10 and 50 cycles when cycled in the voltage range 0.005−1.5 and 0.005−3 V, respectively. The structural and morphological evolutions during cycling and their implications on the Li-cycling behavior of Zn_2SnO_4 nanowires are examined. The effect of the choice of voltage range and initial morphology of the active material on the Li-cycleabilty is also elucidated.

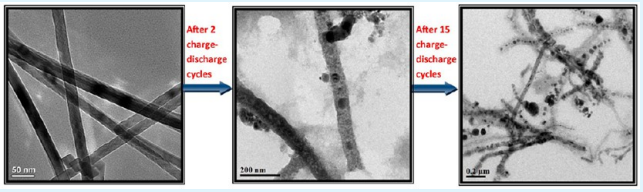

KEYWORDS: *Zn_2SnO_4 nanowires, Zn_2SnO_4 nanoplates, Li-cycling, morphological dependence, anodes, lithium ion batteries*

INTRODUCTION

Lithium ion batteries (LIBs) are widely used as rechargeable power sources for various consumer electronics appliances because it is lightweight and efficient compared to other electrochemical systems such as Ni-MH batteries.[1] LIBs are considered as a prospective energy storage device to power the future plug-in electric hybrid vehicles (PHEVs) and EVs, which require high power and energy density.[2] Graphite and lithium titanate ($Li_4Ti_5O_{12}$), which are used as the anode material for commercial Li-ion rechargeable batteries, cannot accomplish the requirement for higher storage capacity due to its low theoretical capacity of 175 and 372 mAh g^{-1}, respectively. Li alloy forming elements (M = Sn, Si, Sb, Ge, Zn, Al, In, Bi, Cd, etc.) are considered as prospective anode materials because of their ability to reversibly react with large amount of Li thereby delivering high capacity at relatively low voltage vs Li.[3] Among Li alloying elements, Sn and Si are the most relevant with a theoretical capacity of 990 and 4200 mAh g^{-1}, respectively, forming $Li_{4.4}M$ alloy. Poizot et al.[4] achieved a breakthrough by demonstrating the reversibility of displacement reaction of transition metal (TM) oxides with lithium, which is termed as "conversion reaction". Upon lithiation or electrochemical reduction of TM oxides, nanometer scale metallic clusters will be dispersed in amorphous Li_2O matrix and thus all possible oxidation states of compound can be utilized during charging, to achieve high reversible capacity.

Sn-based oxides, such as SnO_2, SnO, and its composites (SnO VO_x, SnO_2−MoO_3), have received special attention as prospective anode materials for LIBs because of their ability to undergo both alloying/dealloying and conversion reaction thereby delivering high capacity values of 600−800 mAh g^{-1}.[5,6] The alloying of Li directly into bulk tin metal causes a large volume expansion, producing cracking of the electrode and rapid loss of capacity. The issue of capacity fading can be addressed by various approaches: (i) Using some counter (matrix) elements in conjunction with the alloy−forming anode, but at the cost of achievable reversible capacity.[7] (ii) Choice of proper voltage range keeping a trade-off between capacity value and capacity stability.[8] (iii) Decreasing the size to nanometer range so that relatively low number of atoms per grain leads to less volume change upon cycling thus reducing the mechanical strain generated within the particles comparison to micrometer-size particles.[1,7](iv) Fabricating 1D nanostructures such as nanowires as electrode materials to provide better accommodation of strain and efficient electron transport through an anisotropic 1D pathway, in addition to benefits of the nanoscale dimensions.[9] Park et al.[10] fabricated 1D SnO_2 nanowires by thermal evaporation process and compared its electrochemical properties with that of SnO_2 powders in the range of 0.005−1.5 V. SnO_2 nanowires showed better Li-cycling behavior with initial discharge capacity of 1134 mAh g^{-1}, which fades to 220 mAh g^{-1} after 50 cycles. Paek et al.[11]

Received: March 4, 2013
Accepted: June 5, 2013
Published: June 5, 2013

synthesized SnO_2 graphene nanosheet composite (SnO_2/GNS) and studied Li-cycling properties were carried out in the voltage range of 0.005−2 V. A reversible capacity of 810 mAh g^{-1} was obtained with capacity retention of 70% after 15 cycles whereas specific capacity of bare SnO_2 nanoparticles dropped to 60 mAh g^{-1} after 15 cycles.

Zinc has been proven to be a good matrix element for conversion based oxides since it can contribute to capacity by alloying-dealloying reaction besides buffering the volume variation.[12,13] Belliard et al.[14] investigated the electrochemical performance of ball-milled ZnO-SnO_2 composite and found that the cycling performance of the electrode was improved when a small amount of ZnO was added into the composites. Wang et al.[15] developed SnO_2/ZnO nanowire array on Cu substrates and cycled in the voltage range 0.005−2.0 V at a current of 120 mA g^{-1}. SnO_2/ZnO composite nanowire array showed a large reversible capacity of 556 mAh g^{-1} after 30 cycles and better cycling performance compared to that of SnO_2 nanotubes,[16] SnO_2 hollow spheres,[17] SnO_2 nanoparticles,[15] and ZnO nanowires.[15] A composite ternary oxide of Zn and Sn, Zn_2SnO_4, which has an inverse spinel structure, received much interest because of its application in gas sensors, dye-sensitized solar cells, and photoelectrochemical cells.[18−20] Previous studies on the Li-cycling behavior of Zn_2SnO_4 showed that upon insertion of Li-ions, its inverse spinel structure collapses and metallic Sn and Zn as well as Li−Sn and Li−Zn alloys is formed.[21,22] It can be concluded that the crystal structure destruction and huge unit cell volume variation accompanied by the conversion and alloying/dealloying reaction can cause capacity loss during cycling. Rong et al.[22] prepared Zn_2SnO_4 nanoparticles by hydrothermal method and studied its electrochemical properties in the voltage range of 0.005−3 V. It delivered an initial discharge capacity of 1384 mAh g^{-1} which faded to 580 mAh g^{-1} after 50 cycles.

In the present work, 1D Zn_2SnO_4 nanowires (NWs) are synthesized directly on stainless steel substrates by a vapor transport method and tested as anodes for lithium ion batteries. Its Li-cycling properties are compared with that of hydrothermally prepared Zn_2SnO_4 nanoplates in two different voltage ranges: 0.005−3 and 0.005−1.5 V. Ex situ TEM studies of Zn_2SnO_4 NW electrode clearly show the swelling of nanowires during initial discharge−charge cycles and its subsequent disintegration into nanoparticles, initiating a gradual capacity fading after first 10 cycles. Nanowires showed better capacity stability during initial cycles, whereas nanoplates exhibited improved performance after first 15 cycles.

EXPERIMENTAL SECTION

Zn_2SnO_4 NWs were synthesized by a vapor transport method involving cocarbothermal reduction of ZnO and SnO_2, using a horizontal tube furnace. A mixture of ZnO, SnO_2, and graphite powders were used as source powder, which was positioned at the closed end of a quartz tube. Stainless steel substrates were placed nearer to the open end of the quartz tube. The small quartz tube was inserted into a large alumina tube, which was sealed and heated to 900 °C at a rate of 20 °C min^{-1} and held for 30 min in an argon/1% oxygen atmosphere with a flow rate of 80 sccm. The base pressure was 10^{-2} mbar, and process pressure was 2 mbar during NW growth. After growth, the furnace was allowed to cool down naturally in Ar atmosphere. Zn_2SnO_4 nanoplates were prepared via hydrothermal route using Na_2CO_3 as mineralizer, adopting a method reported by Annamalai et al.[23] The compounds were characterized by powder X-ray diffraction (XRD) (Philips X'PERT MPD, Cu Kα) and high resolution transmission electron microscope (HR-TEM) (JEOL JEM 2010 operating at 200 kV). For transmission electron microscopy (TEM) studies, the powder samples of the as-synthesized Zn_2SnO_4 were dispersed in ethanol using ultrasonic mixing.

For ex-situ TEM studies, the electrodes were recovered by dismantling the cells inside the glovebox, washed with dimethyl carbonate (DMC) and the materials were scratched out. Ethanol solution containing Zn_2SnO_4 NWs/nanoplates was dropped onto copper TEM grids with supporting carbon films. Stainless steel substrates coated with Zn_2SnO_4 NW were directly used as electrodes for Li-cycling. The weight of the active material is calculated using high sensitive microbalance, Shimadzu Libror AEM-5200 model. Coin-type test cells (size 2016) were assembled in an argon-filled glovebox (MBraun, Germany) using Li metal (Kyokuto Metal Co., Japan) foil as counter electrode, glass microfiber filter (GF/F, Whatman Int.Ltd., Maidstone, England) as the separator and 1 M $LiPF_6$ in ethylene carbonate (EC) and DMC (1:1 by volume, Merck Selectipur LP40) as the electrolyte. Electrode preparation procedure adopted for Zn_2SnO_4 nanoplates was discussed elsewhere.[24] The cyclic voltammetry and galvanostatic discharge−charge cycling of the cells were carried out at room temperature (25 °C) by computer controlled MacPile II (Biologic, France) unit and Bitrode multiple battery tester (model SCN, Bitrode, U.S.A.), respectively.

RESULTS AND DISCUSSIONS

XRD patterns of Zn_2SnO_4 nanowires (on stainless steel substrate) and nanoplates are shown in Figure 1a and 1b,

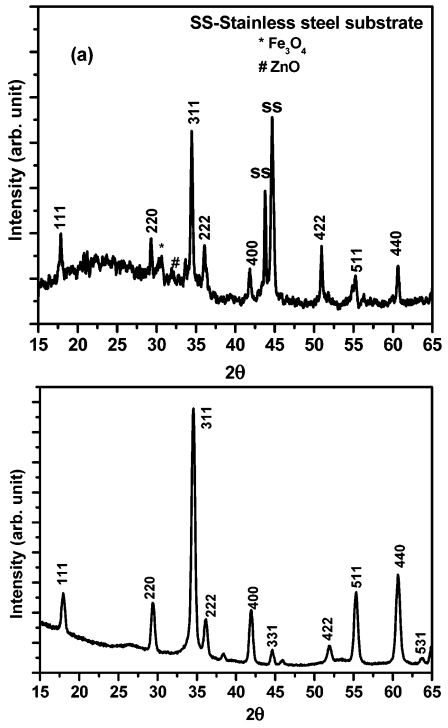

Figure 1. X-ray diffraction (XRD) patterns [Cu Kα radiation] of (a) Zn_2SnO_4 nanowires on stainless steel substrate. (b) Hydrothermally prepared Zn_2SnO_4 nanoplates. Miller indices are shown. 2θ in degrees.

respectively. Except the lines due to stainless steel (SS) substrate, the positions of the main peaks of Zn_2SnO_4 nanowires XRD pattern are consistent with JCPDS data (74−2184) of face centered spinel-structured Zn_2SnO_4 with a space group of Fd3m and lattice parameter of a = 8.650 Å. An impurity line corresponding to Fe_3O_4 (18%) can be seen at 30.4° which is initiated from the SS substrate due to oxidation of Fe, during the synthesis. Figure 2a shows a low-magnification TEM image of the Zn_2SnO_4 nanowires. The synthesized

dx.doi.org/10.1021/am400802j | ACS Appl. Mater. Interfaces 2013, 5, 6054−6060

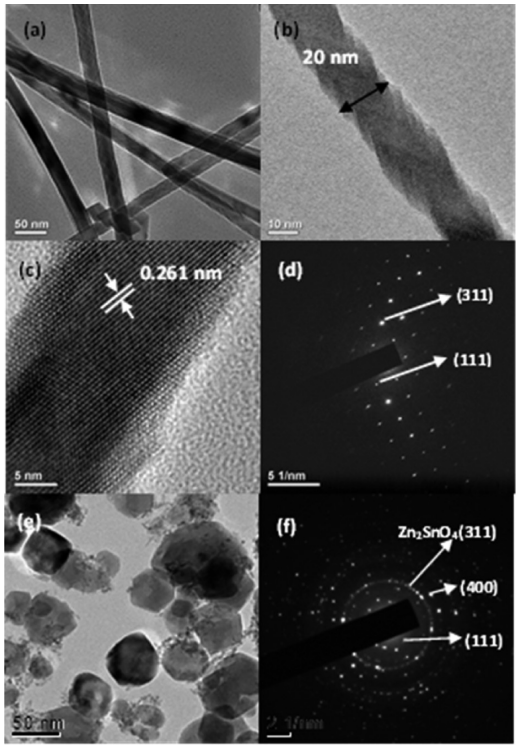

Figure 2. TEM photograph of (a) Zn_2SnO_4 nanowires. Scale is 50 nm. (b) Zn_2SnO_4 nanowires. Scale is 10 nm. (c) HRTEM lattice image of Zn_2SnO_4 nanowires. Scale is 5 nm. (d) SAED pattern of Zn_2SnO_4 nanowires. (e) TEM photograph of Zn_2SnO_4 nanoplates. Scale is 50 nm. (e) SAED pattern of Zn_2SnO_4 nanoplates.

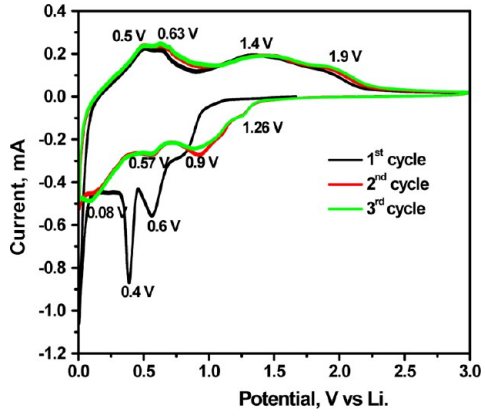

Figure 3. Cyclic voltammogramm of Zn_2SnO_4 nanowire electrode. Potential window, 0.005−3.0 V; scan rate, 58 μV s^{-1}. Li metal was the counter and reference electrode.

nanowires have uniform diameters of 20−30 nm, and their lengths extend up to 10 μm (not fully captured in the image). As opposed to many conventional types of nanowires that present smooth surface morphologies, the most striking observation is that these nanowires exhibit periodic surface morphologies. A magnified TEM image focusing on a single Zn_2SnO_4 nanowire is shown in Figure 2b. Close examination reveals that the nanowire is formed through the self-assembly and fusing of a chain of inlaid rhombohedral crystals such that regular steps with a step size of about 10 nm develop on the nanowire surface. Chen et al.[25] and Wang et al.[26] observed periodically twinned Zn_2SnO_4 nanowires during their TEM investigation on Zn_2SnO_4 nanowires synthesized by the vapor

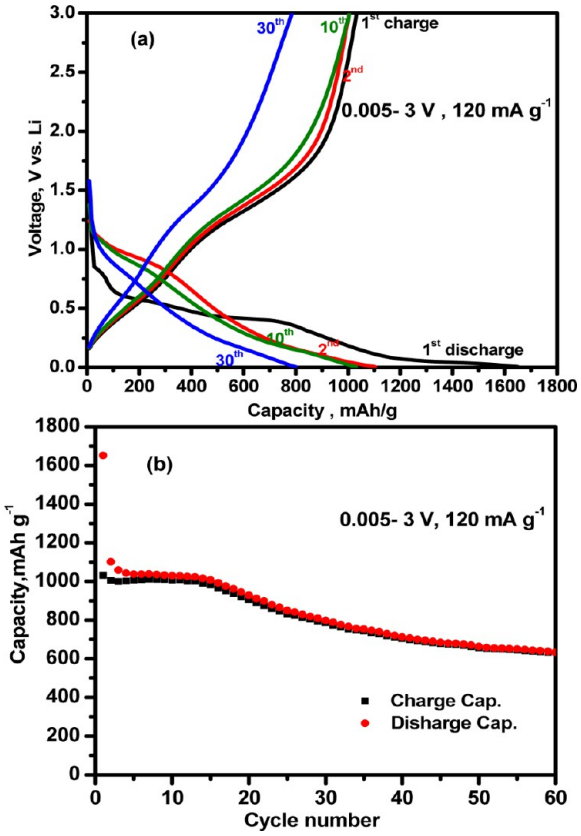

Figure 4. (a) Voltage vs capacity profiles of Zn_2SnO_4 NW electrodes. (b) Capacity vs cycle number plot for Zn_2SnO_4 NW electrodes. Voltage range: 0.005−3 V vs Li. Current: 120 mA g^{-1}.

transport method. The HRTEM lattice image of NWs is shown in Figure 2c and the measured interplanar spacings match well with the *d*-value (0.260 nm) corresponding to the (311) plane of Zn_2SnO_4. The selected area electron diffraction pattern (SAED) in Figure 2d consists of bright spots with (111) and (311) planes indicated. Nanoplate-like morphology of the hydrothermally prepared Zn_2SnO_4 sample is well evident from Figure 2e and the corresponding SAED pattern (Figure 2f) consists of bright spots superimposed on diffuse rings indicating nanocrystalline nature of the sample. The interplanar distances (*d*-values) corresponding to these spots/rings are derived by averaging the displacement of two symmetric spots/rings about the central (000) spot in reciprocal space and subsequently converting them to real space dimensions. The derived *d*-values are attributable to the (111), (311), and (400) planes of cubic-Zn_2SnO_4.

Cyclic voltammetry is carried out in the voltage range of 0.005−3 V, to identify the mechanism of the Li-cycling of Zn_2SnO_4 nanowire electrodes, with Li-metal acting as the counter and reference electrode. Figure 3 represents the cyclic voltammogram (CV) of the first three cycles of Zn_2SnO_4 nanowire electrodes cycled in the range of 0.005−3 V, at the rate of 58 μV s^{-1}. First cathodic scan shows two major peaks at 0.6 and 0.4 V and a sharp peak at 0.05 V, which corresponds to the formation of solid electrolyte interphase (SEI) because of the reduction of solvents in the electrolyte, crystal structure destruction (eq 1) followed by Li-alloying of Sn and Zn (eq 2 and 3), respectively.

$$Zn_2SnO_4 + 8Li \rightarrow 2Zn + Sn + 4Li_2O \quad (1)$$

dx.doi.org/10.1021/am400802j | ACS Appl. Mater. Interfaces 2013, 5, 6054−6060

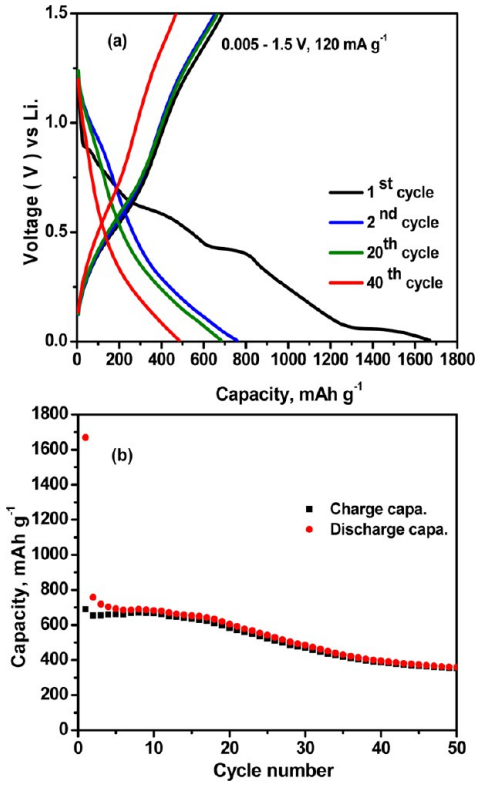

Figure 5. (a) Voltage vs capacity profiles of Zn_2SnO_4 NW electrodes. (b) Capacity vs cycle number plot for Zn_2SnO_4 electrodes. Voltage range: 0.005- 1.5 V vs Li; current: 120 mA g^{-1}.

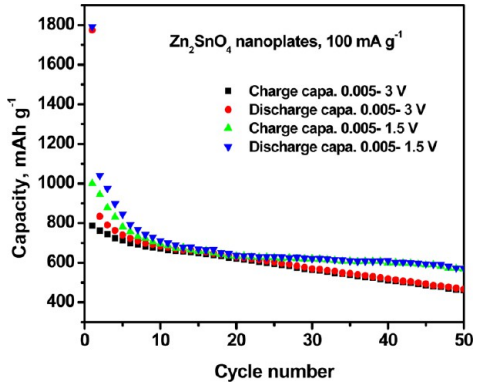

Figure 6. Capacity vs cycle number plot for Zn_2SnO_4 nanoplate electrodes. Current: 120 mA g^{-1}.

$$Sn + 4.4Li \leftrightarrow Li_{4.4}Sn \quad (2)$$

$$2Zn + 2Li \leftrightarrow 2LiZn \quad (3)$$

The peaks at 0.4 and 0.6 V disappear in subsequent cathodic cycles and three smaller peaks are emerged at 0.57, 0.9, and 1.26 V. The absence of the peaks at 0.6 and 0.4 V from second cycle onward indicates the irreversibility of initial lithiation procees (eq 1) and the SEI formation. According to Wang et al.,[27] Li−Zn alloy formation occurs at 0.35 V and multistep dealloying process of Li−Zn alloy occurs in the range of 0.5−0.8 V vs Li. The dealloying/alloying reaction of $Li_{4.4}Sn$ takes place in the voltage range of 0.3−0.5 V versus Li.[7,28] So during the anodic scan, the peaks at 0.5 and 0.63 V correspond to dealloying reaction of Sn and Zn. It is clear from the previous studies that Sn metal is converted to Sn^{2+} at 1.3 V (eqn.4) whereas the oxidation of Sn^{2+} to Sn^{4+} and Zn^0 to Zn^{2+} (eq 5 and 6) happens above 1.5 V.[10,29−31]

The peaks at 1.4 and 1.9 V in the anodic curve can be assigned to conversion reaction of Sn to SnO and eventually to SnO_2 as in eqs 4 and 5. The redox couple 0.9/1.4 V is attributed to the conversion reaction of SnO and 0.08 V/0.5 V and 0.57/0.63 V corresponds to Li-alloying−dealloying reaction of Sn and Zn, respectively (eq 2, 3, and 4). It is noticeable from the cyclic voltammetry studies that the conversion of SnO to SnO_2 and Zn to ZnO can be excluded if we restrict the upper cutoff voltage to 1.5 V.

$$Sn + Li_2O \leftrightarrow SnO + 2Li \quad (4)$$

$$SnO + Li_2O \leftrightarrow SnO_2 + 2Li \quad (5)$$

$$Zn + Li_2O \leftrightarrow ZnO + 2Li \quad (6)$$

Galvanostatic cycling studies of Zn_2SnO_4 nanowires and nanoplates are carried out in two voltage ranges; 0.005−3 and 0.005−1.5 V at the current rate of 120 mA g^{-1} to examine the effect of voltage range on Li-cycling performance. The charge−discharge profiles of the Zn_2SnO_4 NWs in the voltage range 0.005−3 and 0.005−1.5 V are shown in Figures 4a and Figure 5a, respectively. First discharge capacity of ∼1650 mAh g^{-1} is obtained in both the voltage ranges. During first discharge, the cell voltage steeply drops to 0.9 V. Then, three plateau-like steps at ∼0.9, 0.6, and 0.4 V can be noticed, yielding a capacity of ∼1260 mAh g^{-1} corresponding to an uptake of 14.7 mols of Li per formula unit. This can be ascribed to the structural destruction upon Li insertion, subsequent formation of nano-Zn and Sn in Li_2O matrix, accompanied with the uptake of 8 mols of Li per formula weight as shown in eqn.1. As-formed metallic Sn and Zn nanodomains undergo alloying reaction with Li to form Li−Sn, Li−Zn alloy phases evident from the extra capacity of 420 mAh g^{-1} obtained below 0.2 V. Theoretical capacity yielded by the alloying-dealloying of Li with Zn and Sn is 547 mAh g^{-1}, which corresponds to 6.4 mols of Li per formula weight of Zn_2SnO_4. But first discharge capacity, 1650 mAh g^{-1}, obtained is higher than the theoretical capacity of 1232 mAh g^{-1}, which corresponds to 14.4 mols of Li according to eq 1, 2, and 3.Excess capacity can be regarded as originating from the presence of Fe_3O_4 impurity, decomposition of the solvent in the electrolyte and subsequent formation of solid electrolyte interphase. It should be noted that the reformation of Zn_2SnO_4 structure is not plausible after the deep discharge, that is, up to 0.005 V.

During the charging up to 3 V, a smooth voltage profile is observed til 0.7 V, which is followed by upward sloping voltage plateau up to ∼2 V and a steep rise up to 3.0 V. Upon charging, the electrochemical dealloying process will be followed by the conversion reaction of Sn to Sn^{4+} and Zn to Zn^{2+}, yielding a higher reversible capacity of 1000 mAh g^{-1}. The achievable theoretical capacity limit upon charging to 3 V is 1061 mAh g^{-1}, which corresponds to 12.4 mols of Li as per eqs 2−6. The respective capacity-cycle no. plot is shown in Figure 4(b). A reversible capacity of 1000 mAh g^{-1} is maintained for 10 cycles and thereafter fades to 695 mAh g^{-1} after 40 cycles with a capacity fading of 30% between 10 and 50 cycles. So in the voltage range of 0.005−3 V, the Li-reaction mechanism occurs via conversion reaction of ZnO and SnO_2 along with the alloying/dealloying of Sn and Zn. The unit cell volume of the lithiated products (after deep discharge) $Li_{22}Sn_5$ and LiZn are 7739 and 242 $Å^3$, whereas that of delithiated products (after

dx.doi.org/10.1021/am400802j | ACS Appl. Mater. Interfaces 2013, 5, 6054−6060

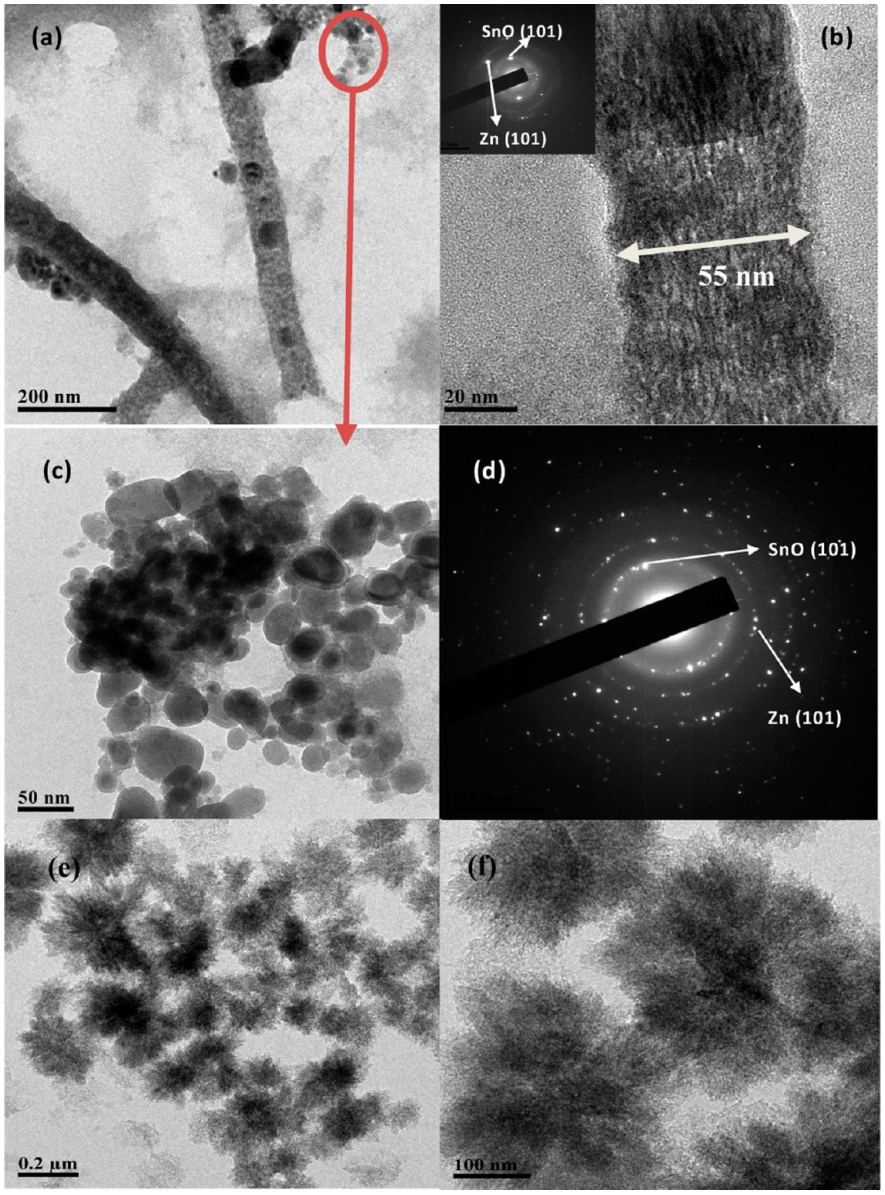

Figure 7. Zn_2SnO_4 nanowire electrode charged to 1.5 V after 2 cycles. (a) TEM image of the cycled nanowires. Scale bar is 100 nm. (b) TEM image of the cycled nanowires. Scale bar is 20 nm. Inset shows the SAED pattern and selected Miller indices. (c) TEM image of the nanoparticles formed from cycled nanowire electrode. Scale bar is 50 nm. (d) SAED pattern of circled region in (c). SnO and Zn along with Miller indices are indicated. (e) Zn_2SnO_4 nanoplate composite electrode charged to 1.5 V after 2 cycles. Scale bar is 0.2 μm. (f) Zn_2SnO_4 nanoplate composite electrode charged to 1.5 V after 2 cycles. Scale bar is 100 nm.

charge to 3 V) SnO_2 and ZnO are 72 and 48 $Å^3$, respectively. So the reactions shown in eqs 2−6 are accompanied by a large unit cell volume variation which finally leads to a detachment of active material.

If the upper potential limit is restricted to 1.5 V, the oxidation of SnO to SnO_2 and Zn to ZnO can be circumvented thereby reducing the unit cell volume variation at the cost of achievable capacity. A total of 8.4 mols of Li is involved in the conversion reaction of SnO (eq 4) and alloying−dealloying of Sn and Zn (eq 5 and 6) with a theoretical capacity of 719 mAh g^{-1}. The first discharge and charge capacities values are 1670 and 690 mAh g^{-1}, respectively. Figure 5b shows the capacity versus cycle no plot of the electrodes cycled in the range of 0.005−1.5 V. A reversible capacity of 670 mAh g^{-1} is obtained which remains constant for first 10 cycles and thereafter starts decreasing. After 50 cycles, a capacity value of 385 mAh g^{-1} is retained which is higher than the theoretical capacity of conventional graphite electrode. Li-cycling behavior of Zn_2SnO_4 NWs is compared with that of nanoplates in both the voltage ranges. The capacity vs cycle number plot derived from galvanostatic charge−discharge profiles of Zn_2SnO_4 nanoplates are shown in Figure 6.

In the voltage range 0.005−1.5 V, it shows a first discharge capacity of 1800 mAh g^{-1} and rapidly fades to 700 mAh g^{-1} by 10 cycles. Capacity retention of 80% is obtained between 10 and 50 cycles. On the other hand, when cycled up to 3 V, a reversible capacity of 670 mAh g^{-1} is achieved after 10 cycles which gradually fades to 470 mAh g^{-1} after 50 cycles with capacity retention of 70% between 10 and 50 cycles. Zn_2SnO_4 nanoplates shows superior electrochemical performance to that of hydrothermally prepared Zn_2SnO_4/C composite reported by Yuan et al.[32] and Zn_2SnO_4 microcubes prepared by Zhu et al.[33]

dx.doi.org/10.1021/am400802j | ACS Appl. Mater. Interfaces 2013, 5, 6054−6060

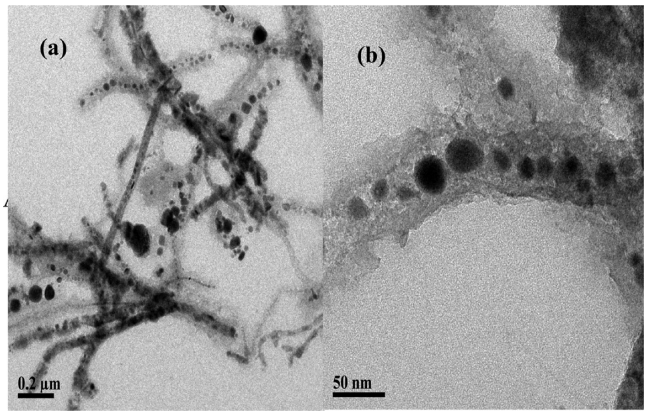

Figure 8. TEM image of Zn_2SnO_4 NW electrode charged to 1.5 V after 15 cycles. (a) Scale bar is 0.2 μm. (b) Scale bar is 50 nm.

According to Yuan et al.,[32] carbon can provide a highly conductive medium for electron transfer, improving the cycling capability. However, Zn_2SnO_4 nanoplates show better Li-storage performance even without carbon coating.

To investigate the morphology and microstructure of the products formed upon Li-cycling; the material was recovered from the nanowire electrodes charged to 1.5 V, after second and 15th charge−discharge cycles. HR-TEM and SAED studies were carried out and the results are shown in Figure 7. After the second charge to 1.5 V (Figure 7a−d), the width of the nanowires increased to ∼55 nm (as-synthesized nanowires were 20 nm in width) and nanoparticles of size 40 nm started forming from the wires. The interplanar distance evaluated from the SAED pattern (inset of Figure 7b) matches well with the d value of (101) plane of SnO and (101) plane of Zn. Thus it is confirmed from SAED patterns of the cycled sample (Figure 7d and inset of Figure 7b) that upon charging to 1.5 V, the electrochemical dealloying process takes place and the intermetallics formed during discharge process get continuously separated in to Li, Sn and Zn nanodomains. The as-formed nano-Sn could be oxidized to SnO at a voltage of around 1.35 V but the Zn remained intact since oxidation of Zn to ZnO occurred just above 1.5 V.[13,30] Figure 7e and 7f show the TEM image of Zn_2SnO_4 nanoplates after second charge to 1.5 V. Zn_2SnO_4 nanoplates were transformed into interconnected nanoflowers after 2 discharge−charge cycles. Figure 8 shows the ex-situ TEM images of electrode material after 15 cycles, charged to 1.5 V. It can be seen that nanowires have been completely broken down into nanoparticles of size ∼40 nm.

During the initial cycles, one-dimensional nanowire-like morphology of the electrode material can buffer the huge volume variation due to crystal structure destruction, alloying dealloying reaction and conversion reaction. After first 2 cycles, the width of the nanowires is doubled and nanosized particle formation starts along the nanowires (Figure 7a) and by the end of 15 cycles, nanowires are completely broken down into nanoparticles as can be seen in Figure 8.

During the in situ observation of the lithiation of the SnO_2 nanowire, Huang et al.[34] observed the swelling, elongation and spiraling of nanowires upon electrochemical charging. The nanowire had elongated by ∼60%, the diameter expanded by ∼45% and the total volume expanded by about 240%.[34] As observed in the present study, after prolonged charging, the nanowire comprised of small nanocrystals dispersed in an amorphous matrix. Similar phenomenon was noticed by Huang et al. in SnO_2 single nanowire electrode.[34] Radial expansion of nanowires during lithiation can be suppressed in coated nanowires due to the mechanical confinement of coating layers.[35] So the Li-cycling properties of Zn_2SnO_4 NWs can be improved by carbon coating on the nanowire by plasma enhanced chemical vapor deposition or atomic layer deposition. For first 10 charge−discharge cycles, Zn_2SnO_4 nanowire electrode showed fairly stable capacity whereas nanoplate composite electrode showed drastic capacity fading, when cycled in both voltage ranges. The initial capacity fading observed in Zn_2SnO_4 nanoplates electrode can be due to the "formation" or "conditioning" of the electrode taking place during first few cycles, whereby the active material undergoes minor structural rearrangement and makes good electrical contact with the conducting carbon particles in the composite electrode, the current-collector and the liquid electrolyte. This kind of initial capacity fading is observed in ternary oxide materials such as $NiFe_2O_4$, $ZnFe_2O_4$.[13,36]

It should be noted that major drawbacks that hinder the practical application of these oxide electrode materials are voltage polarization and Coulombic inefficiency.[37,38] One of the possible origins for the large voltage hysteresis comes from the large amount of interfacial surface generated in first discharge. Reversibility from first to second discharge cycle can be improved by a new "pseudocapacitive process" occurring at the starting stage of second discharge. It compensates for the loss of capacity due to electrolyte decomposition during first discharge, thus leading to a high Coulombic efficiency. According to Lopez et al.,[38] the design of different morphologies in nanosize and the study of their interfaces can open up new perspectives for understanding conversion based oxide anode materials.

CONCLUSIONS

In summary, self-supported Zn_2SnO_4 NW on stainless steel electrodes are fabricated and its electrochemical performances are compared with hydrothermally synthesized Zn_2SnO_4 nanoplates, in two voltage windows 0.005−3 and 0.005−1.5 V. For the first few cycles, Zn_2SnO_4 NW electrodes showed fairly stable capacity, whereas Zn_2SnO_4 nanoplates composite electrode showed drastic capacity fading. In the voltage range 0.005−3 V, nanowire electrode retains a capacity of 660 mAh g^{-1} after 50 cycles and in the lower cut off voltage of 1.5 V, a capacity of 390 mAh g^{-1} is delivered after 50 cycles. The capacity fading behavior observed in Zn_2SnO_4 NW electrodes, after 10 cycles, can be attributed to the complete destruction of nanowires into nanoparticles and eventual disconnection from the stainless steel substrate during further cycling. For Zn_2SnO_4 nanoplate electrodes, the "formation" or "conditioning" of the electrode happen for first 10 cycles and capacity stability of 70% and 80% is achieved between 10 and 50 cycles, in the voltage range 0.005−3.0 and 0.005−1.5 V, respectively. It can be also concluded that an upper cut off voltage of 1.5 V is better than 3 V to obtain improved capacity stability in Zn_2SnO_4 composite electrode.

AUTHOR INFORMATION

Corresponding Author

*E-mail: physowch@nus.edu.sg.

Notes

The authors declare no competing financial interest.

REFERENCES

(1) Yuan, X., Liu, H., Zhang, J., Eds. *Lithium-Ion Batteries: Advanced Materials and Technologies*; CRC Press: Boca Raton, FL, 2011.
(2) Majeau-Bettez, G.; Hawkins, T. R.; Strømman, A. H. *Environ. Sci. Technol.* **2011**, *45*, 4548−4554.
(3) Park, C.-M.; Kim, J.-H.; Kim, H.; Sohn, H.-J. *Chem. Soc. Rev.* **2010**, *39*, 3115−3141.
(4) Poizot, P.; Laruelle, S.; Grugeon, S.; Dupont, L.; Tarascon, J. M. *Nature* **2000**, *407*, 496−499.
(5) Meduri, P.; Pendyala, C.; Kumar, V.; Sumanasekera, G. U.; Sunkara, M. K. *Nano Lett.* **2009**, *9*, 612−616.
(6) Das, B.; Reddy, M. V.; Subba Rao, G. V.; Chowdari, B. *J. Solid State Electrochem.* **2011**, *15*, 259−268.
(7) Reddy, M. V.; Subba Rao, G. V.; Chowdari, B. V. R. *J. Mater. Chem.* **2011**, *21*, 10003−10011.
(8) Courtney, I. A.; Dahn, J. R. *J. Electrochem. Soc.* **1997**, *144*, 2943−2948.
(9) Chan, C. K.; Peng, H.; Liu, G.; McIlwrath, K.; Zhang, X. F.; Huggins, R. A.; Cui, Y. *Nat. Nano* **2008**, *3*, 31−35.
(10) Park, M. S.; Wang, G. X.; Kang, Y. M.; Wexler, D.; Dou, S. X.; Liu, H. K. *Angew. Chem., Int. Ed.* **2007**, *46*, 750−753.
(11) Paek, S.-M.; Yoo, E.; Honma, I. *Nano Lett.* **2008**, *9*, 72−75.
(12) Sharma, Y.; Sharma, N.; Subba Rao, G. V.; Chowdari, B. V. R. *Adv. Funct. Mater.* **2007**, *17*, 2855−2861.
(13) Cherian, C. T.; Reddy, M.; Subba Rao, G. V.; Sow, C. H.; Chowdari, B. V. R. *J. Solid State Electrochem.* **2012**, *16*, 1823−1832.
(14) Belliard, F.; Connor, P. A.; Irvine, J. T. S. *Solid State Ionics* **2000**, *135*, 163−167.
(15) Wang, J.; Du, N.; Zhang, H.; Yu, J.; Yang, D. *Mater. Res. Bull.* **2011**, *46*, 2378−2384.
(16) Wang, J.; Du, N.; Zhang, H.; Yu, J.; Yang, D. *J. Phys. Chem. C* **2011**, *115*, 11302−11305.
(17) Wu, P.; Du, N.; Zhang, H.; Zhai, C.; Yang, D. *ACS Appl. Mater. Interfaces* **2011**, *3*, 1946−1952.
(18) Tan, B.; Toman, E.; Li, Y.; Wu, Y. *J. Am. Chem. Soc.* **2007**, *129*, 4162−4163.
(19) Alpuche-Aviles, M. A.; Wu, Y. *J. Am. Chem. Soc.* **2009**, *131*, 3216−3224.
(20) Chen, Z.; Cao, M.; Hu, C. *J. Phys. Chem. C* **2011**, *115*, 5522−5529.
(21) Becker, S. M.; Scheuermann, M.; Sepelak, V.; Eichhofer, A.; Chen, D.; Monig, R.; Ulrich, A. S.; Hahn, H.; Indris, S. *Phys. Chem. Chem. Phys.* **2011**, *13*, 19624−19631.
(22) Rong, A.; Gao, X. P.; Li, G. R.; Yan, T. Y.; Zhu, H. Y.; Qu, J. Q.; Song, D. Y. *J. Phys. Chem. B* **2006**, *110*, 14754−14760.
(23) Annamalai, A.; Carvalho, D.; Wilson, K. C.; Lee, M.-J. *Mater. Charact.* **2010**, *61*, 873−881.
(24) Cherian, C. T.; Sundaramurthy, J.; Kalaivani, M.; Ragupathy, P.; Kumar, P. S.; Thavasi, V.; Reddy, M. V.; Sow, C. H.; Mhaisalkar, S. G.; Ramakrishna, S.; Chowdari, B. V. R. *J. Mater. Chem.* **2012**, *22*, 12198−12204.
(25) Chen, H.; Wang, J.; Yu, H.; Yang, H.; Xie, S.; Li, J. *J. Phys. Chem. B* **2005**, *109*, 2573−2577.
(26) Wang, J.; Sun, X. W.; Xie, S.; Zhou, W.; Yang, Y. *Cryst. Growth Des.* **2007**, *8*, 707−710.
(27) Wang, H.; Pan, Q.; Cheng, Y.; Zhao, J.; Yin, G. *Electrochim. Acta* **2009**, *54*, 2851−2855.
(28) Sharma, N.; Plévert, J.; Subba Rao, G. V.; Chowdari, B. V. R.; White, T. J. *Chem. Mater.* **2005**, *17*, 4700−4710.
(29) Li, J.; Zhao, Y.; Wang, N.; Guan, L. *Chem. Commun.* **2011**, *47*, 5238−5240.
(30) Deng, Y.; Zhang, Q.; Tang, S.; Zhang, L.; Deng, S.; Shi, Z.; Chen, G. *Chem. Commun.* **2011**, *47*, 6828−6830.
(31) Aurbach, D.; Nimberger, A.; Markovsky, B.; Levi, E.; Sominski, E.; Gedanken, A. *Chem. Mater.* **2002**, *14*, 4155−4163.
(32) Yuan, W. S.; Tian, Y. W.; Liu, G. Q. *J. Alloys Compd.* **2010**, *506*, 683−687.
(33) Zhu, X. J.; Geng, L. M.; Zhang, F. Q.; Liu, Y. X.; Cheng, L. B. *J. Power Sources* **2010**, *189*, 828−831.
(34) Huang, J. Y.; Zhong, L.; Wang, C. M.; Sullivan, J. P.; Xu, W.; Zhang, L. Q.; Mao, S. X.; Hudak, N. S.; Liu, X. H.; Subramanian, A.; Fan, H.; Qi, L.; Kushima, A.; Li, J. *Science* **2010**, *330*, 1515−1520.
(35) Zhang, L. Q.; Liu, X. H.; Liu, Y.; Huang, S.; Zhu, T.; Gui, L.; Mao, S. X.; Ye, Z. Z.; Wang, C. M.; Sullivan, J. P.; Huang, J. Y. *ACS Nano* **2011**, *5*, 4800−4809.
(36) Vidal-Abarca, C.; Lavela, P.; Tirado, J. L. *J. Phys. Chem. C* **2010**, *114*, 12828−12832.
(37) Reddy, M. V.; Subba Rao, G. V.; Chowdari, B. V. R. *Chem. Rev.* **2013**, DOI: 10.1021/cr3001884.
(38) Lopez, M. C.; Ortiz, G. F.; Lavela, P.; Alcantara, R.; Tirado, J. L. *ACS Sustainable Chem. Eng.* **2013**, *1*, 46−56.